
Article:
Tan, S. orcid.org/0000-0002-5556-5821 and Hand, R.J. (2018) Incorporation and phase separation of Cl in alkaline earth aluminosilicate glasses. Journal of Nuclear Materials, 507. pp. 135-144. ISSN 0022-3115

https://doi.org/10.1016/j.jnucmat.2018.04.044

Incorporation and phase separation of Cl in alkaline earth aluminosilicate glasses

Shengheng Tan and Russell J. Hand[1]
ISL, Department of Materials Science and Engineering, University of Sheffield, Sir Robert Hadfield Building, Mappin Street, S1 3JD, Sheffield, UK

Abstract:

Pyrochemical reprocessing of spent nuclear fuels may lead to the generation of chloride containing wastes. ^{36}Cl wastes may also arise from the treatment of irradiated graphite. Such wastes will have limited solubility in the borosilicates currently used for waste vitrification. Despite requiring higher processing temperatures aluminosilicate glasses show promise for this application. In a series of alkaline earth aluminosilicate glasses we demonstrate that chloride solubility is related to the alkaline earth species as follows Sr > Sr+Ba > Ba > Ca > Mg, with the strontium aluminosilicate glass accommodating up to 5.92 at% Cl. Typical chloride retention rates are ~80% of the batched chloride content at 1400ºC. It has also been observed that, when Cl is present in the glass in excess, phase separation firstly occurs as formation of non-Cl crystals (mainly alkaline earth aluminosilicates, with a minority of aluminates); a segregated chloride layer is only formed at higher chlorine loadings. This indicates that chlorine solubility in glass is not only controlled by the capacity of glass network to accommodate Cl^- but also by the stability of glass network after Cl^- incorporation. In addition, increased incorporation of Cl^- in glass results in steadily decreased glass densities and glass transition temperatures.

Keywords: Chlorine, aluminosilicate, glass, phase separation

[1] Corresponding author r.hand@sheffield.ac.uk

1. Introduction

Chloride containing wastes may arise from the pyrochemical reprocessing of nuclear fuels [1-3]. In addition long-lived ^{36}Cl is a problematic isotope in irradiated graphite (i-graphite) which in some processing scenarios could be separated from and thus immobilised independently of the i-graphite [4, 5]. While, in principle, the non-radioactive Cl from pyrochemical reprocessing wastes could be allowed to evolve from the melt and go into the off-gas, this will lead to a large off-gas stream with subsequent secondary processing requirements [6, 7]. The compatibility of Cl with the borosilicate glasses conventionally used for nuclear waste immobilisation is low and thus it is desirable to identify alternative glass compositions for the immobilisation of such wastes [8-10]. Siwadamrongpong *et al.* [11] working on immobilisation of municipal solid wastes that contain sources of chloride identified calcium aluminosilicates as potential glasses for the immobilisation of such wastes. More recently Schofield *et al*. [12, 13] examined the possibility of using calcium aluminosilicate glasses for the immobilisation of some simulated pyrochemical reprocessing wastes. In addition, mineralogical studies [14-16] on magmatic glasses, where chlorides are also widely present, have shown that chloride solubility in aluminosilicate glass varies with cation species, although the solubilities are generally low in such glasses.

As part of a wider investigation into the incorporation of anionic species present in waste streams, including Cl^-, SO_4^{2-} and MoO_4^{2-}, we have therefore investigated the use of a range of alkaline earth aluminosilicates and have previously reported the potential of magnesium aluminosilicates for the immobilisation of MoO_4^{2-} [17]. In the current paper we report on the incorporation of chloride into the range of alkaline earth aluminosilicate glasses studied to determine the effects of changing the alkaline earth species on the rate of chloride incorporation, as well as the resultant changes in glass structure and properties caused by chloride addition.

2. Experimental

2.1. Glass making

A family of alkaline earth aluminosilicate (AeAS) glasses with different chlorine loadings were prepared. The glasses had a nominal mole composition of $45SiO_2$-$10Al_2O_3$-$(45–x)$AeO-$x$$AeCl_2$ (Ae = Ba, Sr, Ca, Mg or a 50:50 mixture of Sr:Ba). In the mixed alkaline earth case only the oxide was added as a mixture. The batched glass compositions in atomic percent are given in Table 1; atomic percentages are used to simplify comparison with analysed compositions due to the presence of two different anions in the glass composition. Sample names are of the form *X*AS-*y*Cl where *X* = M, C, S, B for Mg, Ca, Sr, Ba or SB for Sr+Ba respectively and *y* (= 2*x*) is the number of moles of Cl added. The precursors for making glass were high purity glass making sand (SiO_2, Loch Aline sand, Tilcon, UK), aluminium trihydroxide ($Al(OH)_3$, Acros Organics, UK), barium carbonate ($BaCO_3$, Fisher Chemical, UK), strontium carbonate ($SrCO_3$, Fisher Chemical, UK), calcium carbonate ($CaCO_3$, Minfil 11220, UK) and magnesium hydroxide ($Mg(OH)_2$, Fisher Chemical, UK). Chlorine was added as a hydrated alkaline earth chloride ($BaCl_2 \cdot 2H_2O$, $SrCl_2 \cdot 10H_2O$, $CaCl_2 \cdot 6H_2O$ or $MgCl_2 \cdot 2H_2O$ as appropriate; (all Fisher Chemical, UK; laboratory grade). When a chloride salt was added a corresponding reduction in the amount of precursors batched for the alkaline earth oxide was made. In all cases batches to produce about 100 g glass were weighed and fully mixed. The homogenised batches were filled into mullite crucibles at 1400 °C, and held at this temperature for 3 h and poured out into a preheated steel mould to form a bar shaped block. The cast glass was immediately transferred to an annealing furnace in which it was annealed at 700 °C for 1 h and cooled down to room temperature at 1 °C min^{-1}. All of the above procedures were carried out in air. Some attack of the mullite crucibles was observed (see analysed compositions below).

2.2. *Sample characterisation*

The density of the glasses was measured using a Mettler Toledo densimeter which utilises Archimedes' principle with deionised water as the immersion medium. The measurement was repeated five times for each sample and the average result taken.

Crushed sample powders passing a 75 μm sieve were collected for powder X-ray diffraction (XRD; Bruker D2 Phaser X-ray Diffractometer, operating at 30 kV and 10 mA) and differential thermal analysis (DTA; Perkin Elmer STA8000). XRD analysis was conducted using Cu$K\alpha$ radiation, over a 2θ range of 10-70° with 0.05° step size. DTA curves were recorded from room temperature to 1200 °C at 10 °C min^{-1} in a platinum crucible under air.

For Raman spectroscopy a 5 mm thick slice was sectioned from the glass block using a Buehler low speed saw with a diamond blade and with oil as lubricant. The top surface of the slice was ground to 1200 SiC grit, thoroughly rinsed with isopropanol and dried prior to measurement. Raman spectra were recorded with a Renishaw Invia Raman spectrometer equipped with a CCD detector, using a green line (514.5 nm) laser at 20 mW laser power and a ×50 objective. The glasses were scanned between 0 and 2000 cm^{-1}, with a 10 s exposure time and 10 accumulations for each sample. Calibration with silicon was undertaken each time the spectrometer was used. In addition for some samples micro-Raman spectra were recorded with a Horiba Raman Microscope using a green line laser (514.5 nm) and a ×100 objective. In this case glasses were scanned between 0 and 1800 cm^{-1}, with a 20 s exposure time and 10 accumulation for each spot.

The morphologies of the prepared samples were examined by scanning electron microscopy (SEM). Ground sample slices were successively polished using 6, 3 and 1 μm diamond suspensions, followed by carbon coating. SEM observation was performed in an FEI Inspect F microscope using both secondary electron imaging (SEI) and backscattered electron imaging

(BEI). Quantitative compositional analysis and X-ray mapping were carried out with an energy dispersive X-ray (EDS) spectrometer attached to a Hitachi TM3010 SEM. In addition, some glass compositions were measured by X-ray fluorescence (XRF) using a PANalytical Zetium X-ray spectrometer (at 25kV and 160mA); powdered samples were used for this analysis.

3. Results and discussion

3.1. Glass composition and chlorine retention

Table 2 details the glass compositions as measured by EDS and XRF. For EDS at least five randomly selected regions were measured and the average taken. The standard deviation for Si and Cl is within 0.30 at%, for Al is within 0.20 at% and for Sr and Ba is within 0.15 at%. For the results averaged between EDS and XRF, the difference between their measured values was limited (<0.20 at%). Dissolution of mullite in the melts, as well as Cl losses, explains the discrepancies between batched and measured compositions. Significant amounts of Cl have dissolved into the BAS, SBAS and SAS glasses, whereas the Cl contents retained in CAS and MAS are low or zero (the CAS glass was only able to retain up to 1.11 at% Cl while the MAS glasses did not retain any Cl). The highest Cl content, measured by EDS, in a homogeneous glass was 5.92 at% Cl in SAS-20Cl glass, although some phase separated glasses, *e.g.* SAS-25Cl and SBAS-20Cl glasses, had higher Cl contents in their glassy regions. In this work Cl solubility is defined as the maximal amount of Cl that could be dissolved in glass while not causing any visible phase separation. Therefore Cl solubility (at% Cl) in AeAS glasses follows the order of SAS (5.92 at%) > SBAS (4.58 at%) > BAS (2.96 at%) > CAS (1.11 at%) > MAS (0). Although the Cl content continued to increase in the glassy regions of the phase separated SAS, BAS and SBAS glasses, it was not possible to produce a single phase glass with this level of chlorine content, and thus from a practical perspective Cl solubility has been exceeded in these glasses. It can also be seen that the combination of Sr and Ba in SBAS glass resulted in a Cl solubility level between that of SAS and BAS glasses. It is possible that changing

processing conditions *e.g.* melt surface area and temperature could enable enhancement of the measured retention rates however these parameters were not investigated in the current work.

The correlation between measured and batched Cl contents in glasses is plotted in Fig. 1. BAS and SAS glasses not only possess a high Cl solubility but also show a constantly high retention rate of ~80% Cl regardless of Cl addition level up to 9 at% Cl batch addition, even though at the highest levels of addition the glasses become heterogeneous. This high Cl retention rate agrees with the retention rate in a barium silicate ($BaSi_2O_5$) glass reported by Stebbins and Du [16] (1.5 wt% chlorine retained at 1.7 wt% addition, in a closed system), which suggests that strontium and/or barium (alumino-) silicate glasses have a high ability to retain Cl. SBAS glasses, in which Sr and Ba are both present in an ~1:1 ratio, have a Cl retention rate similar to that of the BAS and SAS glasses, unless the Cl addition was very large when a separate chloride layer was formed (SBAS-25Cl). In addition, using different chloride precursors (either $SrCl_2$ or $BaCl_2$) in the batch resulted in insignificant changes in Cl retention behaviour in the glass[2]. Meanwhile the CAS glass shows a Cl retention rate of less than 40% on initial addition of Cl and then reaches saturation at ~1.11 at% Cl. This is much lower than the Cl retention levels reported for CAS glasses by Siwadamarongpong *et al*. [11] and Schofield *et al.* [12], however their glasses contained about 4 mol% less alumina and 4 mol% more calcium than the ones studied here. It is notable that Chen *et al.* [18] have recently reported very significant chloride incorporation in calcium silicate glasses that do not contain alumina[3] and thus it seems likely that if more than a few percent of alumina is present in calcium (alumino-)silicate glasses then their ability to retain chloride is significantly reduced. Although the reasons for this are not entirely clear, Sandland *et al.* [19] have previously found that Cl is associated with modifier

[2] Based on the target glass composition only alkaline earth chlorides were considered as chloride sources in this work, although other chloride sources could be present in actual wastes.
[3] Although reported chloride contents were up to 23.8 at% Cl (estimated) the glasses reacted readily with water and thus would not be suitable for nuclear waste immobilisation.

ions in aluminosilicates rather than aluminium ions; in addition Zimova and Webb [20] have also noted a decrease in chloride content with increasing aluminium content in glass.

As detailed in Table 2, glass density steadily decreases with increasing Cl content in glass, *e.g.* from 3.484 g cm^{-3} for SAS-5Cl glass to 3.412 g cm^{-3} for SAS-20Cl glass and from 3.799 g cm^{-3} for SBAS-5Cl glass to 3.655 g cm^{-3} for SBAS-20Cl glass. Meanwhile Fig. 2 shows that the molar volume of glass exhibits a slight increase on initial incorporation of Cl, followed by a significant increase with further increases in the Cl content in the glass. For example with SAS glass, the molar volume slightly increases from 24.3 cm^3 for SAS-0Cl to 24.7 cm^3 for SAS-10Cl glass, and then linearly increases with further Cl incorporation, finally reaching 26.4 cm^3 for SAS-25Cl glass. Such changes agree with the observations reported in Refs [11] and [21], and are probably related to the ionic size and location of Cl^- ions in glass network: Cl^- ions have a large volume but a low mass. For low Cl incorporation levels there is sufficient free interstitial space in the glass network to accommodate Cl^- ions without causing significant network expansion; the incorporation of Cl^- therefore gives rise to only a slightly increased molar volume. However, as the Cl content in glass increases, further accommodation of Cl^- ions requires notable network expansion, so that the glass molar volume increases significantly corresponding to a decrease in glass density. Thus the greater the amount of Cl that is incorporated, the greater the expansion of the glass network and the lower the glass density.

Figures 3 to 5 show the XRD patterns of SAS, SBAS and BAS glasses, respectively, which exhibit two broad humps indicating that the materials are X-ray amorphous. SAS glass remains XRD amorphous until SAS-25Cl glass which exhibits some inconspicuous crystalline peaks at 2θ = 13.9°, 23.9°, 27.8°, 30.2° and 35.4°. The observed peaks are however not suitable for accurate phase identification, although they agree with the pattern reported for a monoclinic strontium aluminosilicate phase ($SrAl_2Si_2O_8$, PDF-4#00-038-1454). Meanwhile, as seen in Fig. 4, amorphous XRD patterns are obtained for BAS-5Cl and -10Cl glasses while a number of

crystalline peaks are observed in the patterns of BAS-15Cl and -20Cl glasses. The primary crystalline phase in both glasses is likely to be hexagonal celsian ($BaAl_2Si_2O_8$, PDF-4#00-012-0726) according to the peaks at 2θ of 11.5° (001), 22.6° (111), 30.2° (112), 33.9° (130), 34.6° (003), 41.1° (221), 46.6° (004) and 49.2° (203), respectively. Two minor phases may also be present in the samples: a monoclinic celsian phase (PDF-4#00-038-1450) indicated by the peaks at 13.6° (020), 23.4° ($\bar{1}30$) and 26.7° ($\bar{2}20$) 2θ and a hexagonal barium aluminate phase ($BaAl_2O_4$, PDF-4#00-017-0306) indicated by the peaks at 19.4° (200), 28.4° (202), 34.3° (220), 40.1° (222), 45.0° (402) and 54.3° (224) 2θ. From Fig. 5 it can be seen that SBAS-0Cl to -20Cl glasses are X-ray amorphous, even though the SBAS-20Cl glass was visibly heterogeneous. Crystalline peaks are observed for SBAS-25Cl glass, which belong to two phases: peaks at 2θ = 13.7°, 19.4°, 22.9°, 23.5°, 25.3°, 25.8°, 26.8°, 27.4°, 29.6°, 34.9° and 41.6° can be attributed to the (020), (021), (200), ($\bar{1}30$), ($\bar{2}21$), ($\bar{1}12$), ($\bar{2}20$), (040), (131), ($\bar{2}41$), (060) planes of monoclinic celsian phases with Sr-substitution ($Ba_xSr_{1-x}Al_2Si_2O_8$, PDF-4#00-038-1450 to -1454); peaks at 2θ = 16.2° (020), 20.1° ($11\bar{2}$), 30.7° ($21\bar{3}$) and 31.2° ($22\bar{2}$) can be attributed to the orthorhombic $BaCl_2$ (PDF-4#00-024-0094). SBAS-25Cl glass is the only one that contains chloride in the separated phase; however the chloride layer is formed during melting for compositions that produce partially crystallised glasses on cooling.

All of the prepared glasses show similar behaviour when analysed using DTA; two examples (SAS-0Cl and -10Cl, without and with Cl addition) are shown in Fig. 6. The glasses remain thermally stable until above their glass transition temperature (T_g, estimated from the extrapolated onset of the first endothermic peak), followed by two exothermic peaks (centred at T_{c1} and T_{c2}, respectively) at higher temperatures. The Cl additions to the glass do not lead to any new DTA peaks, however they do result in changes in temperatures at which the above thermal reactions take place. As plotted in Fig. 7, T_g shows a linear decrease from 797 °C for the SAS base glass down to 749 °C for SAS-20Cl glass; this trend continues to SAS-25Cl glass

which is slightly phase separated. Such a decrease is likely caused by increasing amounts of chloride clusters in glass network: according to Refs [19, 22], Cl^- ions are present as cation-Cl cluster species in a glass network, making the network more open and destabilised, therefore lowering the energy required for structural relaxation.

The first exothermic peak in DTA curves is an indicative of a crystallisation process and, similar to T_g, T_{c1} exhibits a linear decrease from 938 to 895 °C with increasing Cl content in glass from SAS-0Cl to -25Cl. Based on related work with the MAS base glass composition we suspect that the crystals are alkaline earth aluminosilicates [15] although additional measurements would be required to prove this. Meanwhile, the second exothermic peak (T_{c2}), which is probably due to formation of hexagonal (Sr-)celsian phases [23-25], slightly increases from 1118 to 1131 °C with the initial Cl addition, for SAS-5Cl glass, and afterwards steadily decreases until reaching 1004 °C for SAS-25Cl glass. The decrease in T_{c1} suggests that the glass is more prone to suffer devitrification upon heating when the chlorine content in glass is increased, while the trend in the T_{c2} values suggests that a small amount of Cl in the glass retards the formation of celsian crystals.

3.2. Phase separation caused by Cl addition (XRD, Raman and SEM)

The Raman spectra of BAS, SAS and SBAS glasses are shown in Figures 8 to 10, respectively. The base glasses have three broad Raman bands located at 280-380, 500-600 and 800-1200 cm^{-1} intervals, which can be assigned to various vibrational modes of the structural units of aluminosilicate glass network [26-29]. The notable feature is that the Cl additions do not result in any new Raman bands until the onset of phase separation. As shown in Fig. 8, all of the SAS glasses, including the glassy region of SAS-25Cl glass, exhibit a pattern similar to that for other silicate glasses. The crystallised region of SAS-25Cl glass has a number of sharp Raman peaks, the most prominent one being at 507 cm^{-1} with others at 159, 200, 250 and 477 cm^{-1}, which are probably due to vibrations in monoclinic $SrAl_2Si_2O_8$ crystals; the patterns agree well with

RRUFF database No. R060152 for monoclinic $BaAl_2Si_2O_8$ which has close structural parameters to monoclinic $SrAl_2Si_2O_8$ [30, 31] (the slight shifts in peak positions are due to the difference between Sr^{2+} and Ba^{2+}). As for BAS glasses, new peaks are observed for BAS-15Cl glass at 102 and 405 cm^{-1}, and for BAS-20Cl glass these two peaks increase in intensity, coupled with the emergence of peaks centred at 182, 295, 476, 673, 809, 924, 955 and 998 cm^{-1}, respectively. Such patterns are in good accordance with the characteristic peaks of hexagonal celsian crystals reported in Refs [32, 33]. As for SBAS glasses (shown in Fig. 10), all of the homogeneous glasses and the glassy regions of phase separated samples only exhibit some broad bands which can be assigned to the glass network, while a peak at 1011 cm^{-1} is recorded from the crystallised region of SBAS-20Cl glass and a series of sharp peaks at 112, 188, 313, 433, 658, 864 and 1011 cm^{-1} are observed for the crystallised region in SBAS-25Cl glass. Other measurements (not shown) show that peaks above 300 cm^{-1} cannot be attributed $BaCl_2$ and thus we believe that the majority of these sharp Raman peaks are attributable to the Sr-substituted celsian crystals detected by XRD (see Fig. 5).

BAS glass becomes visibly phase separated at 5.31 and 7.02 at% Cl additions (BAS-15Cl and -20Cl samples respectively), respectively. Needle-like and plate-like particles are widely, but non-uniformly, dispersed within the crystallised region of BAS-15Cl glass, with a width range of 5 to 20 μm and a length up to 100 μm (see Fig. 11*a*). These particles tend to aggregate together in BAS-20Cl glass (Fig. 11*b*), although again they are non-uniformly dispersed, indicating a higher rate of growth of the separated phase with higher Cl additions. In addition, a lighter grey phase (Area E in Fig. 11*b*), which is surrounded by the primary separated phase, can also be observed under SEM. Fig. 12 presents the EDS spectra of the above phases and glass matrices. While a significant amount of Cl is present in both glass matrices (A and C), it is essentially absent from the separated phases B and D. The plate-like crystals (marked as B and D, from BAS-15Cl and -20Cl glasses, respectively) are both stoichiometrically close to

$BaAl_2Si_2O_8$, the formula of celsian which is suggested by Raman and XRD results to be the primary crystalline phase. The separated phase E in BAS-20Cl glass contains limited Si and Cl, with a stoichiometry close to $BaAl_2O_4$, which also agrees with the XRD results.

SBAS glasses begin to phase separate from SBAS-20Cl (7.02 at% Cl addition) and a thin chloride layer is formed on the surface of SBAS-25Cl (8.70 at% Cl addition) in addition to phase separation inside the glass. Again the separated layer formed during melting. As shown in Fig. 13*a*, the separated particles in SBAS-20Cl glass are plate-like and are sparsely distributed within the glass matrix. In a similar fashion to the crystals formed in heterogeneous BAS glasses these plate-like crystals do not contain Cl. The atomic ratios between elements determined by EDS (see Table 3) indicates that the likely formula of these crystals is $Ba_{1-x}Sr_xAl_2Si_2O_8$, where $x \sim 1/3$. Fig. 13*b* shows a fracture surface directly taken from SBAS-25Cl glass, where a chloride layer and some separated particles are both observed. The segregated layer contains a significant amount of Ba and Cl, whereas the separated particles are compositionally similar to those found in the SBAS-20Cl glass, where Sr substitutes for one third of Ba in $BaAl_2Si_2O_8$ composition.

SAS-25Cl glass is the only sample that exhibits phase separation among the SAS glass series, with two phases formed within glass matrix (as seen in Fig. 14*a* and *b*): dark plate-like particles and grey rod-like particles. The plates are generally of 200 μm in length and widely dispersed across the glass, while the rods are much smaller and are only embedded in some of the plates. EDS elemental mapping of an area where both phases are present is shown in Fig. 15. Both phases are enriched in Al, but the plates contain more Si while the rods contain more Sr and a large amount of Cl. As presented in Table 3, the atomic ratio of Sr:Al:Si in the plates is close to 1:2:2, agreeing with that of $SrAl_2Si_2O_8$, the presence of which is also suggested by Raman results. In comparison with the plates, the rods have half the Si content and double the Sr content, as well as about 6 at% Cl. This did not correlate with either the XRD or Raman results.

Therefore in order to further understand the phase separation in SAS-25Cl glass, micro-Raman spectroscopy was used to analyse the crystallised area (Fig. 16). Area J is a glassy region showing a Raman spectrum consistent with the bulk glass. Raman spectra in line with those for monoclinic Sr-celsian were obtained from Areas B, C, F and I. Areas D and E, which are assumed to be the region containing Cl, show distinct spectra with characteristic peaks at 450, 618 and 899 cm^{-1}. These features are in accordance with $SrAl_2O_4$, with the peaks being respectively assigned to the bending modes of O-Al-O bonds, and symmetric stretching modes and asymmetric stretching modes of Al-O-Al bonds in AlO_4^- tetrahedra [34, 35]. Combined with EDS results, a certain amount of Si has been introduced to substitute for Al, possibly together with the incorporation of Cl in $SrAl_2O_4$ lattice. This substitution may be responsible for the Raman peak at ~1000 cm^{-1} due to the presence of Si-O-Si bonds.

In summary, phase separation caused by excess Cl added to AeAS glasses is complicated. It has been observed that phase separation started to occur on cooling as Cl additions to SAS, SBAS and BAS glasses increased, even if the chloride additions were insufficient to cause the formation of a chloride layer on the melt surface. Such separated phases predominantly crystallise in a plate like hexagonal or monoclinic (Sr-substituted) celsian crystals, probably through nucleation and crystal growth on cooling. Compositional analysis indicates that such plates contain a negligible amount of Cl, although these crystals were not formed in the glasses without Cl additions. In the meantime, the Cl content in the glassy region of some phase separated glasses continues to increase, suggesting that removing alumina from the glass composition is beneficial in maximising chlorine retention, in line with the inferences that can be made from the results reported in Refs [11], [12] and [18]. Therefore, it is likely that phase separation in Cl-rich glass is not only driven by the capacity of glass network to accommodate Cl but also by the stability of glass network after Cl incorporation, depending on whichever of the two is reached first. However, there also exists a tiny amount of aluminate crystals in the

separated phases, mostly embedded in the plates. The notable Cl content in them means that Cl indeed is linked with the process of phase separation in these glasses. Both primary aluminosilicate and secondary aluminate crystals are abundant in Al, which implies that micro-heterogeneity of glass, where Al-rich regions are formed, may be an important factor that induces phase separation.

While the work reported here was concentrates on the Cl incorporation limits for the production of homogeneous glasses, a heterogeneous wasteform may be acceptable for final disposal if all the phases present exhibit suitable levels of durability (see, for example, [36]).

4. Conclusions

A series of alkaline earth aluminosilicate glasses with different Cl additions were prepared. The following conclusions are drawn:

(1) SAS, SBAS and BAS glasses are promising for the incorporation of Cl given their excellent Cl retention rate (80%, at 1400°C) for Cl addition levels of up to 9 at%. The highest Cl solubility in a homogeneous glass was 5.92 at% Cl in SAS-20Cl glass. These glasses are therefore potentially attractive for either the immobilisation of chloride containing pyrochemical reprocessing wastes or possibly ^{36}Cl separated from i-graphite.

(2) Cl solubility in glass is determined by both the capacity of the glass network to incorporate Cl and the stability of glass network after Cl incorporation. CAS glass is controlled by the former factor while SAS, SBAS and BAS glasses are controlled by the latter one.

(3) Cl^- ions are initially incorporated into interstitial spaces in the glass network, but further Cl^- incorporation results in significant network expansion. The abundant Cl content in glass may also destabilise glass network, which is probably responsible for the decrease of T_g of the glasses.

(4) Cl^- ions are incorporated in the amorphous structure of the glass; only phase separated glasses show crystalline XRD and Raman peaks.

(5) In SAS and BAS glasses, alkaline earth aluminosilicate crystals are the dominant phases that are firstly separated from glass network when Cl is in excess; a small amount of aluminate crystals can be formed inside the aluminosilicate phases. The dominant separated particles are Cl-free, but the embedded aluminates can contain Cl.

Acknowledgements

ST thanks the "UK-China Scholarship for Excellence" for financial support. This research was performed in part at the MIDAS Facilities at the University of Sheffield, which was established with support from the Department of Energy and Climate Change (UK).

References

[1] B.L. Metcalfe, I.W. Donald, Candidate wasteforms for the immobilization of chloride-containing radioactive waste, J. Non-Cryst. Solids, 348 (2004) 225-229.

[2] S.V. Tomilin, A.N. Lukinykh, A.A. Lizin, A.V. Bychkov, V.V. Yakovlev, V.I. Konovalov, Investigation of the incorporation of spent alkali chloride melt in ceramic, At. Energ., 102 (2007) 217-222.

[3] E.R. Vance, J. Davis, K. Olufson, I. Chironi, I. Karatchevtseva, I. Farnan, Candidate waste forms for immobilisation of waste chloride salt from pyroprocessing of spent nuclear fuel, J. Nucl. Mater., 420 (2012) 396-404.

[4] TECDOC-1790, Processing of Irradiated Graphite to Meet Acceptance Criteria for Waste Disposal, INTERNATIONAL ATOMIC ENERGY AGENCY, Vienna, 2016.

[5] A. Wickham, H.-J. Steinmetz, P. O'Sullivan, M.I. Ojovan, Updating irradiated graphite disposal: Project 'GRAPA' and the international decommissioning network, J. Environ. Radioact., 171 (2017) 34-40.

[6] M.I. Ojovan, W.E. Lee, An Introduction to Nuclear Waste Immobilisation, Elsevier, Amsterdam, 2005.

[7] I.W. Donald, Waste immobilisation in glass and ceramic based hosts: radioactive, toxic and hazardous wastes, John Wiley & Sons, Ltd, Chichester, UK, 2010.

[8] M.I. Ojovan, O.G. Batyukhnova, Glasses for nuclear waste immobilisation, in: WM'07 Conference, Tucson AZ, 2007.

[9] I.W. Donald, B.L. Metcalfe, S.K. Fong, L.A. Gerrard, D.M. Strachan, R.D. Scheele, A glass-encapsulated calcium phosphate wasteform for the immobilization of actinide-, fluoride-, and chloride-containing radioactive wastes from the pyrochemical reprocessing of plutonium metal, J. Nucl. Mater., 361 (2007) 78-93.

[10] N.S. Ilyukhina, I.Y. Panomaryova, T.N. Lashchenova, S.V. Stefanovsky, Solubility of Sulfate and Chloride Ions in Borosilicate Melts at Vitrification of Intermediate-Level Radioactive Wastes, in: WM2010 Conference, Phoenix, 2010.

[11] S. Siwadamrongpong, M. Koide, K. Matusita, Prediction of chloride solubility in CaO–Al_2O_3–SiO_2 glass systems, J. Non-Cryst. Solids, 347 (2004) 114-120.

[12] J.M. Schofield, P.A. Bingham, R.J. Hand, The Immobilisation of a Chloride Containing Actinide Waste Surrogate in Calcium Aluminosilicate Glasses, in: A. Cozzi, T. Ohji (Eds.) Environmental Issues and Waste Management Technologies in the Materials and Nuclear Industries XII, John Wiley & Sons, Inc., 2009, pp. 69-80.

[13] J. Schofield, Vitrification of a chloride containing actinide waste surrogate, in: Department of Materials Science and Engineering, the University of Sheffield, Sheffield, UK, 2011.

[14] J.D. Webster, R.J. Kinzler, E.A. Mathez, Chloride and water solubility in basalt and andesite melts and implications for magmatic degassing, Geochim. Cosmochim. Acta, 63 (1999) 729-738.

[15] J.D. Webster, B. De Vivo, Experimental and modeled solubilities of chlorine in aluminosilicate melts, consequences of magma evolution, and implications for exsolution of hydrous chloride melt at Mt. Somma-Vesuvius, Am. Mineral., 87 (2002) 1046-1061.

[16] J.F. Stebbins, L.S. Du, Chloride ion sites in silicate and aluminosilicate glasses A preliminary study by ^{35}Cl solid-state NMR, Am. Mineral., 87 (2002) 359-363.

[17] S. Tan, M.I. Ojovan, N.C. Hyatt, R.J. Hand, MoO_3 incorporation in magnesium aluminosilicate glasses, J. Nucl. Mater., 458 (2015) 335-342.

[18] X. Chen, N. Karpukhina, D.S. Brauer, R.G. Hill, High chloride content calcium silicate glasses, Phys. Chem. Chem. Phys., 19 (2017) 7078-7085.

[19] T.O. Sandland, L.S. Du, J.F. Stebbins, J.D. Webster, Structure of Cl-containing silicate and aluminosilicate glasses: A ^{35}Cl MAS-NMR study, Geochim. Cosmochim. Acta, 68 (2004) 5059-5069.

[20] M. Zimova, S. Webb, The effect of chlorine on the viscosity of Na_2O-Fe_2O_3-Al_2O_3-SiO_2 melts, Am. Mineral., 91 (2006) 344-352.

[21] A.A. Kiprianov, N.G. Karpukhina, Oxyhalide silicate glasses, Glass Phys. Chem., 32 (2006) 1-27.

[22] K.A. Evans, J.A. Mavrogenes, H.S. O'Neill, N.S. Keller, L.Y. Jang, A preliminary investigation of chlorine XANES in silicate glasses, Geochem. Geophy. Geosy., 9 (2008) 15.

[23] N.P. Bansal, M.J. Hyatt, C.H. Drummond, Crystallization and Properties of Sr-Ba

Aluminosilicate Glass-Ceramic Matrices, in: J.B. Wachtman (Ed.) Proceedings of the 15th Annual Conference on Composites and Advanced Ceramic Materials: Ceramic Engineering and Science Proceedings, John Wiley & Sons, Inc., 1991, pp. 1222-1234.

[24] W.E. Lee, M. Chen, P.F. James, Crystallisation of celsian ($BaAl_2Si_2O_8$) glass, J. Am. Ceram. Soc., 78 (1995) 2180-2186.

[25] B. Liguori, C. Ferone, S. Anaclerio, C. Colella, Monoclinic Sr-celsian by thermal treatment of Sr-exchanged zeolite A, LTA-type framework, Solid State Ionics, 179 (2008) 2358-2364.

[26] D.A. Mckeown, F.L. Galeener, G.E. Brown, Raman Studies of Al Coordination in Silica-Rich Sodium Aluminosilicate Glasses and Some Related Minerals, J. Non-Cryst. Solids, 68 (1984) 361-378.

[27] P.F. McMillan, Raman-Spectroscopy in Mineralogy and Geochemistry, Annu. Rev. Earth Planet. Sci., 17 (1989) 255-283.

[28] D.R. Neuville, B.O. Mysen, Role of aluminium in the silicate network: In situ, high-temperature study of glasses and melts on the join SiO_2-$NaAlO_2$, Geochim. Cosmochim. Acta, 60 (1996) 1727-1737.

[29] D.R. Neuville, L. Cormier, V. Montouillout, P. Florian, F. Millot, J.C. Rifflet, D. Massiot, Amorphous materials: Properties, structure, and durability: Structure of Mg- and Mg/Ca aluminosilicate glasses: ^{27}Al NMR and Raman spectroscopy investigations, Am. Mineral., 93 (2008) 1721-1731.

[30] M.M. Krzmanc, M. Valant, D. Suvorov, The synthesis and microwave dielectric properties of $Sr_xBa_{1-x}Al_2Si_2O_8$ and $Ca_yBa_{1-y}Al_2Si_2O_8$ ceramics, J. Eur. Ceram. Soc., 27 (2007) 1181-1185.

[31] D. Long-González, J. López-Cuevas, C.A. Gutiérrez-Chavarría, P. Pena, C. Baudin, X. Turrillas, Synthesis of monoclinic Celsian from Coal Fly Ash by using a one-step solid-state reaction process, Ceram. Int., 36 (2010) 661-672.

[32] J.I. Eldridge, K.N. Lee, Phase Evolution of Bsas in Environmental Barrier Coatings, in: M. Singh, T. Jessen (Eds.) 25th Annual Conference on Composites, Advanced Ceramics, Materials, and Structures: B: Ceramic Engineering and Science Proceedings, The American Ceramic Society, Cocoa Beach, Florida, 2001, pp. 383-390.

[33] A. Kremenovic, P. Colomban, B. Piriou, D. Massiot, P. Florian, Structural and spectroscopic characterization of the quenched hexacelsian, J. Phys. Chem. Solids, 64 (2003) 2253-2268.

[34] U. Rodehorst, M.A. Carpenter, S. Marion, C.M.B. Henderson, Structural phase transitions and mixing behaviour of the Ba-aluminate ($BaAl_2O_4$)—Sr-aluminate ($SrAl_2O_4$) solid solution, Mineral. Mag., 67 (2003) 989-1013.

[35] Y.L. Chang, H.I. Hsiang, M.T. Liang, Phase evolution during formation of $SrAl_2O_4$ from $SrCO_3$ and alpha-Al_2O_3/AlOOH, J. Am. Ceram. Soc., 90 (2007) 2759-2765.

[36] M.I. Ojovan, W.E. Lee, Glassy Wasteforms for Nuclear Waste Immobilization, Metall. Mater. Trans. A, 42 (2010) 837-851.

Table 1 Batched glass compositions in atomic %

Sample	Si	Al	Sr	Ba	Cl	O
SAS-5Cl	16.22	7.21	16.22	-	1.80	58.56
SAS-10Cl	16.07	7.14	16.07	-	3.57	57.14
SAS-15Cl	15.93	7.08	15.93	-	5.31	55.75
SAS-20Cl	15.79	7.02	15.79	-	7.02	54.39
SAS-25Cl	15.65	6.96	15.65	-	8.70	53.04
SBAS-5Cl	16.22	7.21	7.66	8.56	1.80	58.56
SBAS-10Cl	16.07	7.14	7.14	8.93	3.57	57.14
SBAS-15ClS	15.93	7.08	9.29	6.64	5.31	55.75
SBAS-15Cl	15.93	7.08	6.64	9.29	5.31	55.75
SBAS-20Cl	15.79	7.02	6.14	9.65	7.02	54.39
SBAS-25Cl	15.65	6.96	5.65	10.00	8.70	53.04
BAS-5Cl	16.22	7.21	-	16.22	1.80	58.56
BAS-10Cl	16.07	7.14	-	16.07	3.57	57.14
BAS-15Cl	15.93	7.08	-	15.93	5.31	55.75
BAS-20Cl	15.79	7.02	-	15.79	7.02	54.39
Sample	**Si**	**Al**	**Mg**	**Ca**	**Cl**	**O**
MAS-5Cl	16.22	7.21	16.22	-	1.80	58.56
MAS-10Cl	16.07	7.14	16.07	-	3.57	57.14
CAS-10Cl	16.07	7.14	-	16.07	3.57	57.14
CAS-20Cl	15.79	7.02	-	15.79	7.02	54.39
CAS-25Cl	15.65	6.96	-	15.65	8.70	53.04
CAS-30Cl	15.52	6.90	-	15.52	10.34	51.72
CAS-35Cl	15.38	6.84	-	15.38	11.97	50.43

Table 2 Analysed glass compositions (at%) measured by EDX and XRF.

Sample	**Si**	**Al**	**Sr**	**Ba**	**Cl**	**O**	**Total**	**Density (g cm^{-3})**
SAS-5Cl	16.12	7.08	16.65	-	1.31	58.84	100.00	3.484±0.001
SAS-10Cl	16.56	6.54	16.25	-	2.92	57.73	100.00	3.475±0.002
SAS-15Cl$^{€}$	16.16	6.27	16.93	-	3.95	56.69	100.00	3.452±0.004
SAS-20Cl	16.48	6.10	16.18	-	5.92	55.32	100.00	3.412±0.012
SAS-25Cl*	16.12	6.20	16.35	-	6.90	54.44	100.01	3.371±0.009
SBAS-5Cl	16.66	6.49	9.28	7.25	1.47	58.85	100.00	3.799±0.002
SBAS-10Cl$^{€}$	16.45	6.55	8.98	7.45	2.88	57.70	100.00	3.752±0.002
SBAS-15ClS	16.03	6.54	8.71	7.92	4.58	56.22	100.00	3.717±0.001
SBAS-15Cl$^{€}$	16.34	6.11	8.93	7.86	4.28	56.49	100.00	3.711±0.002
SBAS-20Cl*	16.03	5.85	8.71	8.35	6.30	54.75	100.00	3.655±0.001
SBAS-25Cl*	17.19	5.84	8.79	6.80	5.28	56.10	100.00	-
BAS-5Cl	16.56	7.55	-	15.38	1.36	59.15	100.00	3.999±0.009
BAS-10Cl$^{€}$	16.52	7.32	-	15.32	2.96	57.87	100.00	3.954±0.011
BAS-15Cl*	17.71	6.89	-	13.78	4.24	57.39	100.00	3.881±0.014
BAS-20Cl*	17.59	6.77	-	13.75	5.61	56.28	100.00	3.795±0.012
	Si	Al	Ca	Mg	Cl	O	Total	
MAS-5Cl*	16.14	8.70	-	14.91	<0.1	60.25	100.00	-
MAS-10Cl*	17.94	7.82	-	13.32	<0.1	60.92	100.00	-
CAS-10Cl	16.85	9.14	13.07	-	0.89	60.05	100.00	2.779±0.001
CAS-20Cl	17.10	9.09	12.73	-	1.06	60.02	100.00	2.772±0.001
CAS-25Cl	16.95	9.32	12.66	-	1.08	59.99	100.00	2.767±0.002
CAS-30Cl	17.18	9.10	12.58	-	1.11	60.03	100.00	2.762±0.002
CAS-35Cl*	17.39	8.77	12.64	-	1.25	59.95	100.00	2.749±0.001

$^{€}$ These samples were analysed by both EDX and XRF, average taken.

* Samples are phase separated and the compositions are taken from the glassy regions.

Table 3 Compositions (at%, by EDX) of separated particles in SAS, SBAS and BAS glasses.

Glass	Sample	Si	Al	Sr	Ba	Cl	O	Total
BAS-	15Cl	15.78	15.39	-	7.04	0.17	61.61	100.00
	20Cl	15.78	15.49	-	6.95	0.06	61.72	100.00
	20Cl(E)	1.74	26.04		14.58	1.00	56.63	100.00
SBAS-	20Cl	14.85	15.82	2.70	5.25	0.00	61.38	100.00
	25Cl	14.97	15.28	2.74	5.70	0.00	61.31	100.00
SAS-	25Cl(P)	15.47	14.80	8.28	-	0.11	61.35	100.00
	25Cl(S)	7.61	16.79	16.10	-	5.99	53.51	100.00

*BAS-20Cl (E) stands for the Area E in BAS-20Cl glass as marked in Fig. 11*b*.
*SAS-25Cl (P) and (S) stands for the plate-like (primary) and stick-like (secondary) separated particles in SAS-25Cl glass, respectively.

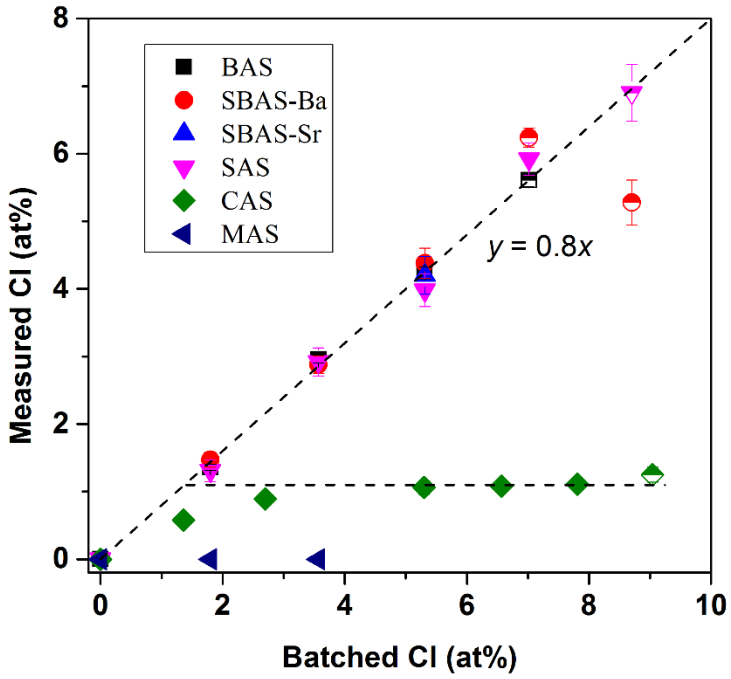

Fig. 1 Correlation between measured and batched Cl content (at%) in glass. Glasses with phase separation are denoted by half-filled symbols. The SBAS-25Cl glass that lies significantly below the $y = 0.8x$ line was the only glass where a separate chloride layer was observed.

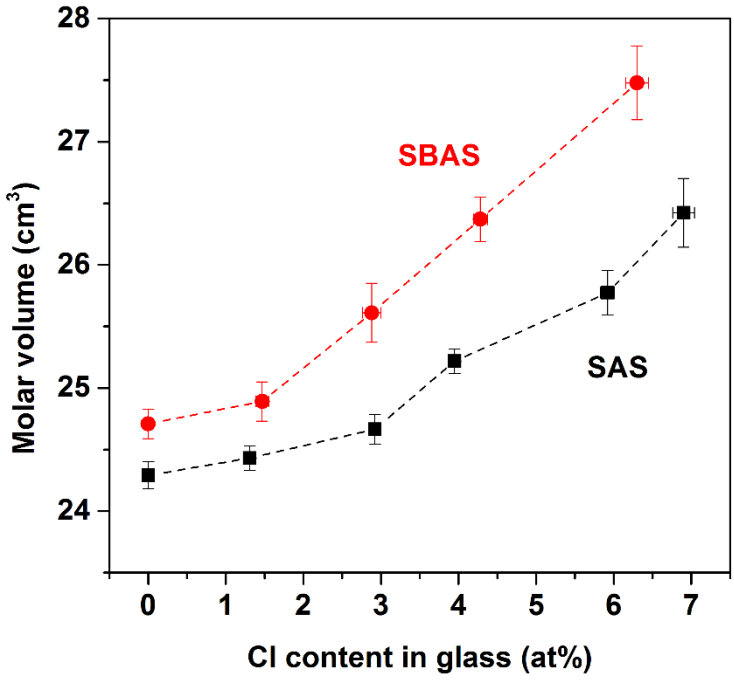

Fig. 2 Molar volume as a function of measured Cl content in the glass.

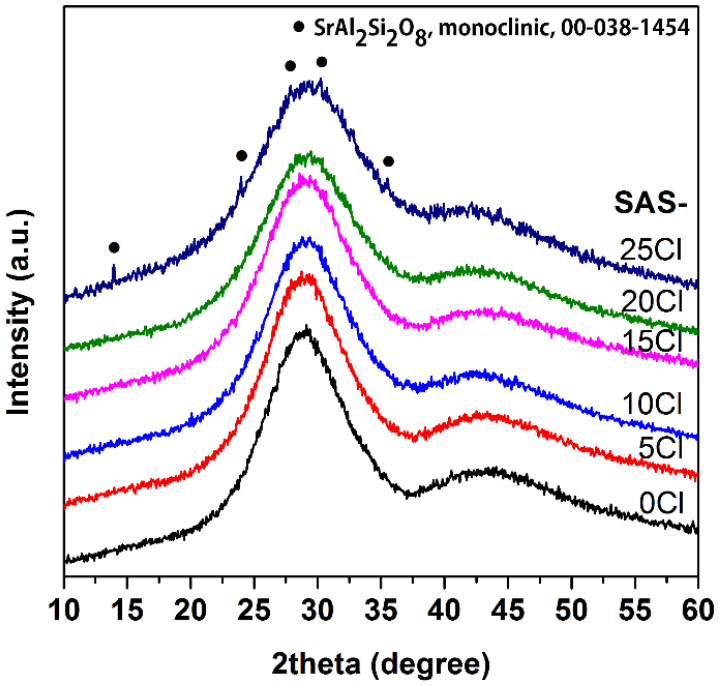

Fig. 3 XRD patterns of SAS glass with Cl additions.

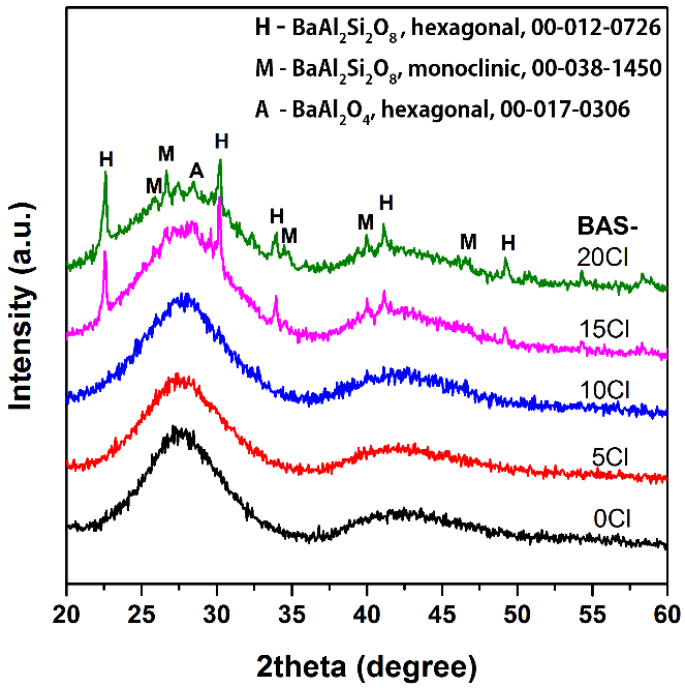

Fig. 4 XRD patterns of BAS glass with Cl additions.

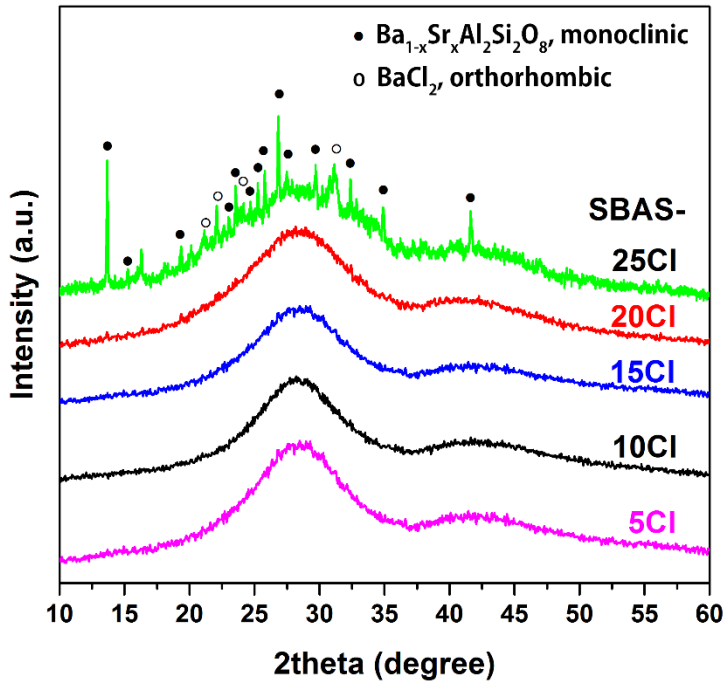

Fig. 5 XRD patterns of SBAS glass with Cl additions

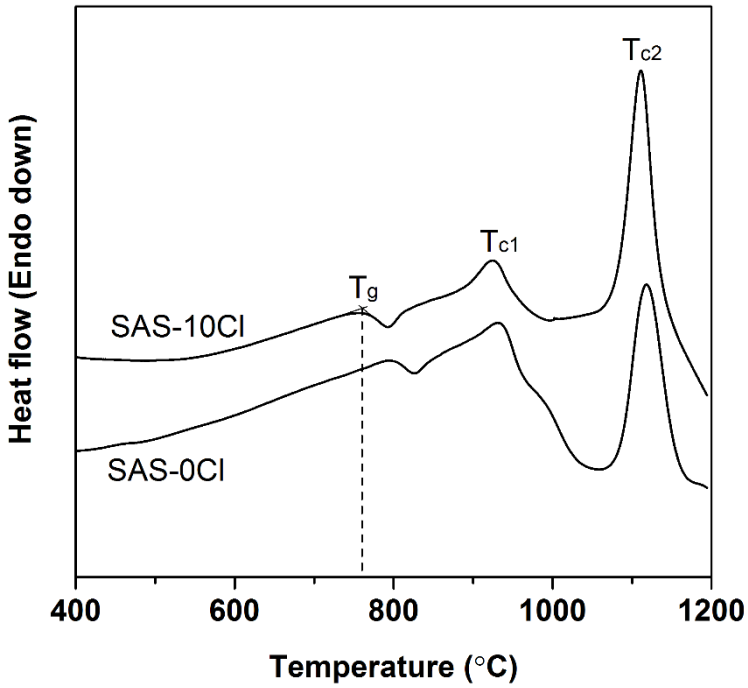

Fig. 6 DTA curves for SAS-0Cl and -10Cl glasses. These are typical of all the DTA curves obtained.

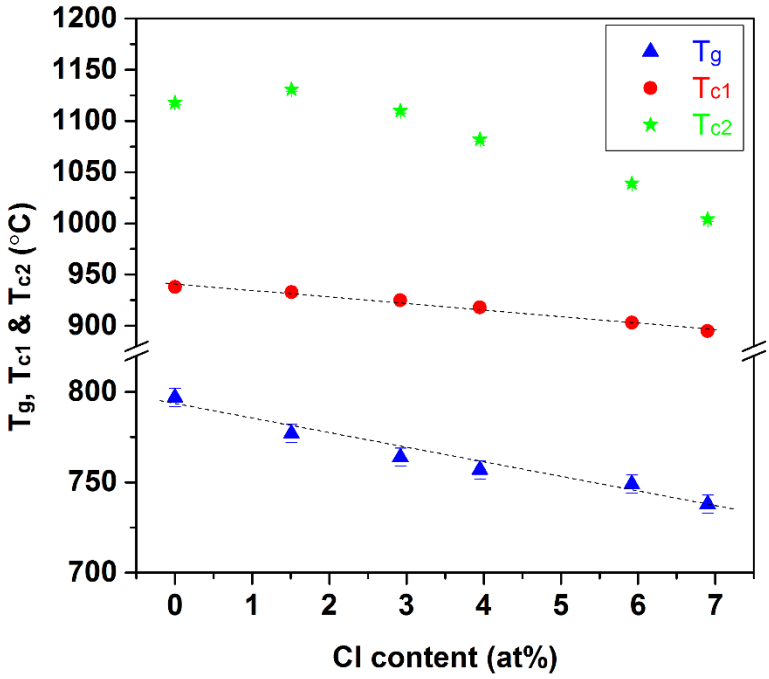

Fig. 7 The change of T_g, T_{c1} and T_{c2} with increasing Cl content in SAS

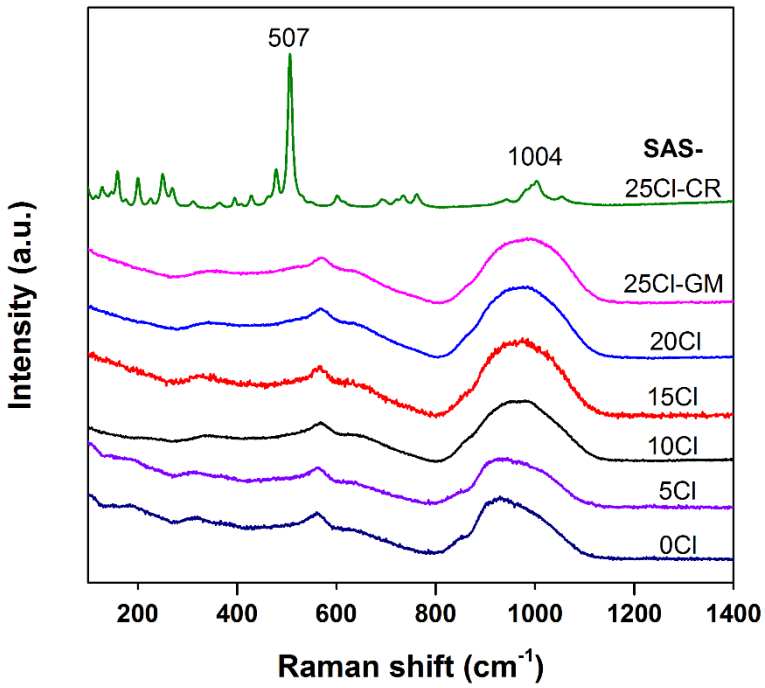

Fig. 8 Raman spectra of SAS glass with Cl additions. GM and CR means the spectrum is from glass matrix and crystallised region, respectively, hereafter the same.

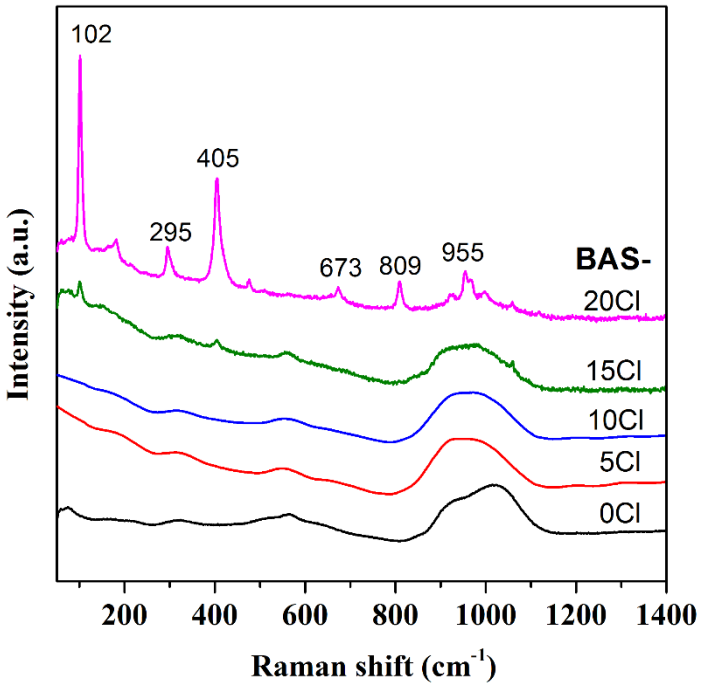

Fig. 9 Raman spectra of BAS glass with Cl additions.

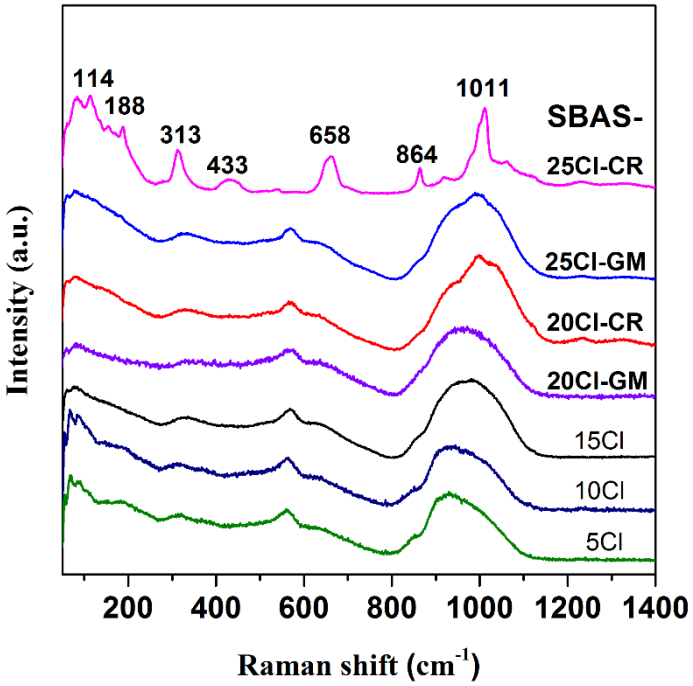

Fig. 10 Raman spectra of SBAS glass with Cl additions.

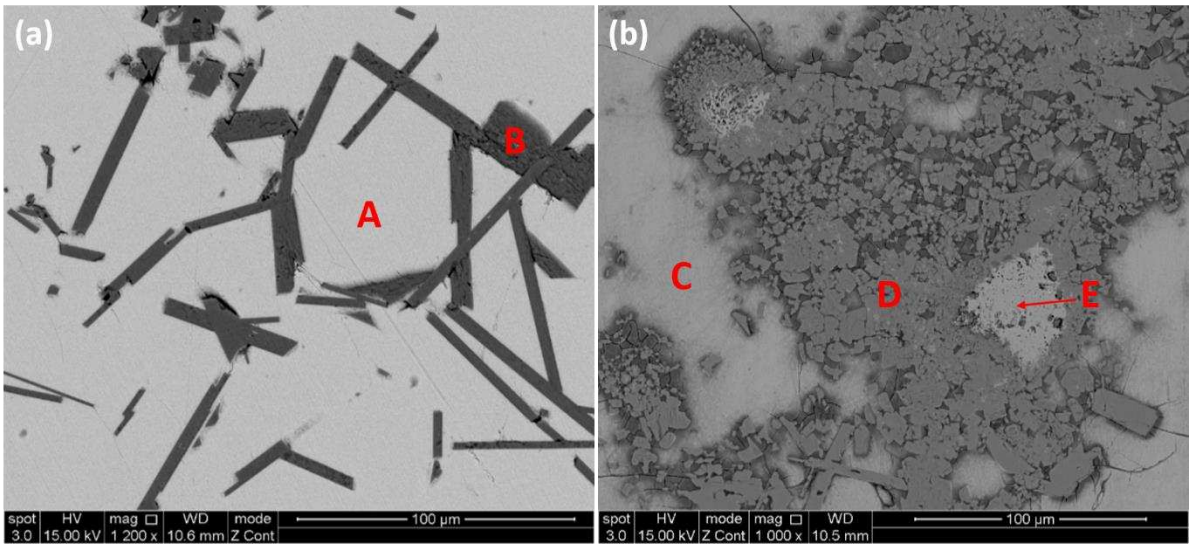

Fig. 11 BSE images of separated particles in (*a*) BAS-15Cl and (*b*) BAS-20Cl glasses, respectively.

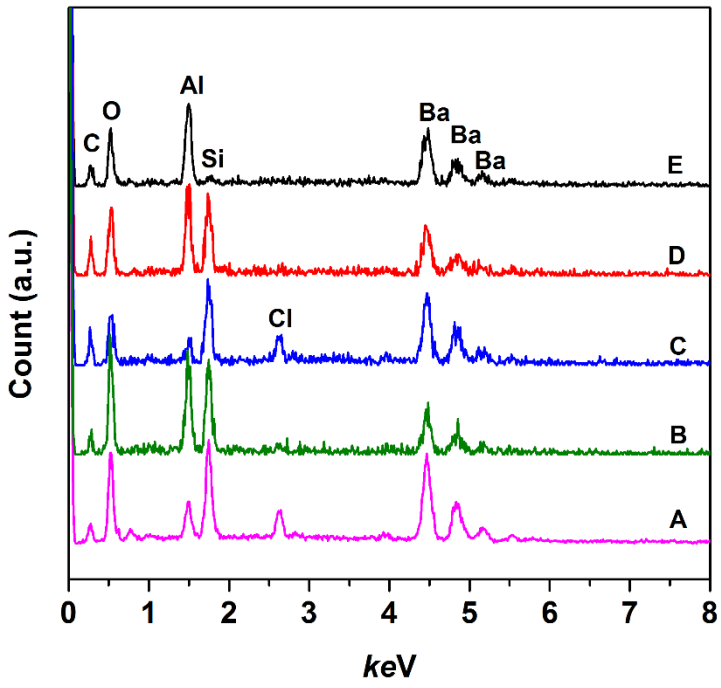

Fig. 12 EDX spectra of different regions (Referred to Fig. 11) in BAS-15Cl and -20Cl glasses.

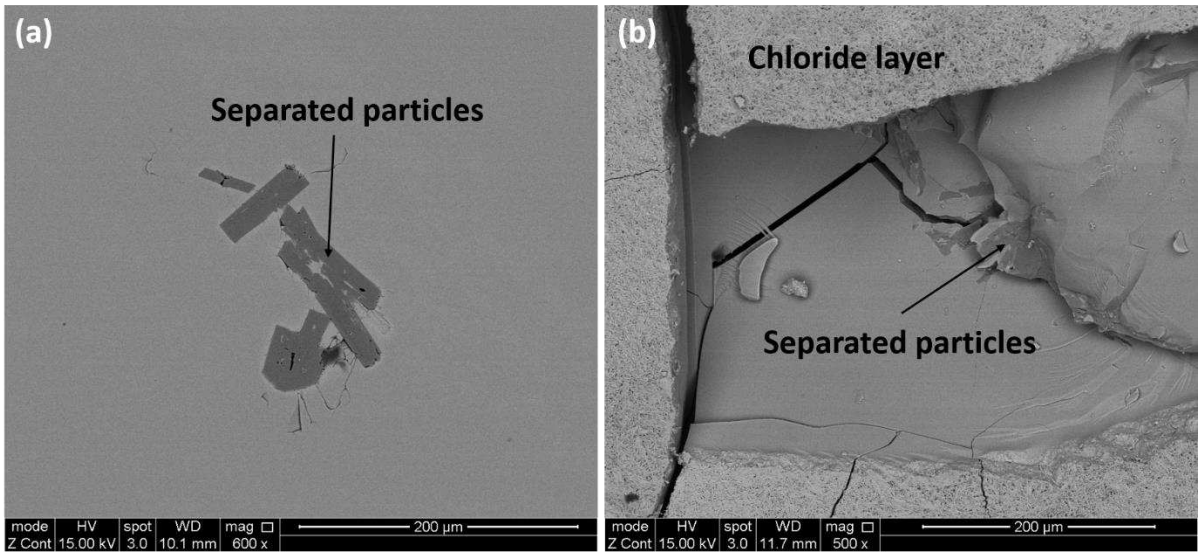

Fig. 13 BSE images of (*a*) SBAS-20Cl and (*b*) SBAS-25Cl glasses.

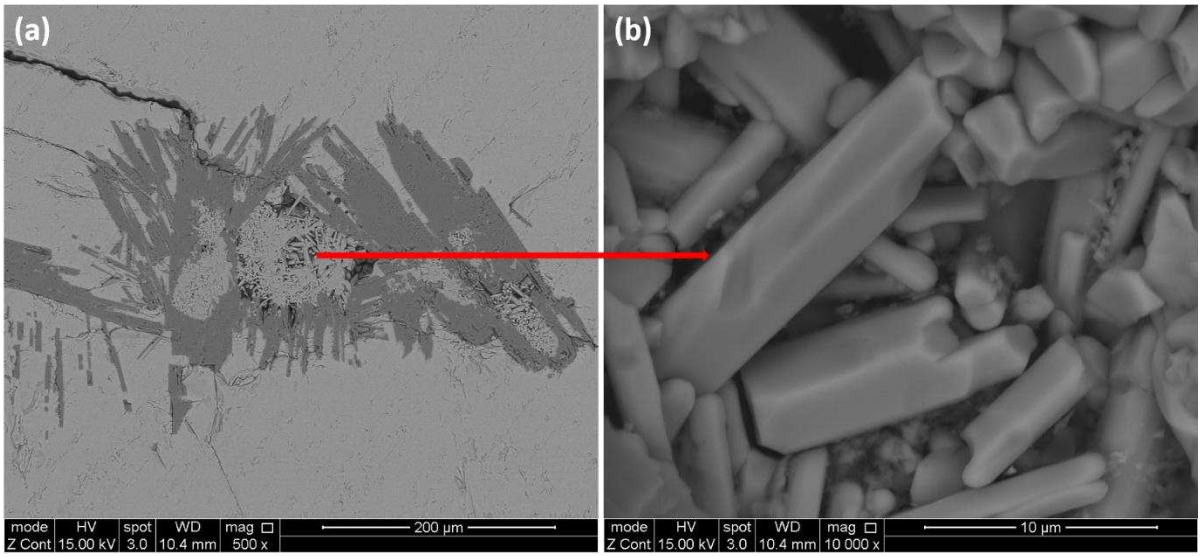

Fig. 14 BSE images of (*a*) separated phases in SAS-20Cl glass and (*b*) rod-like particles embedded in the primary separated phases.

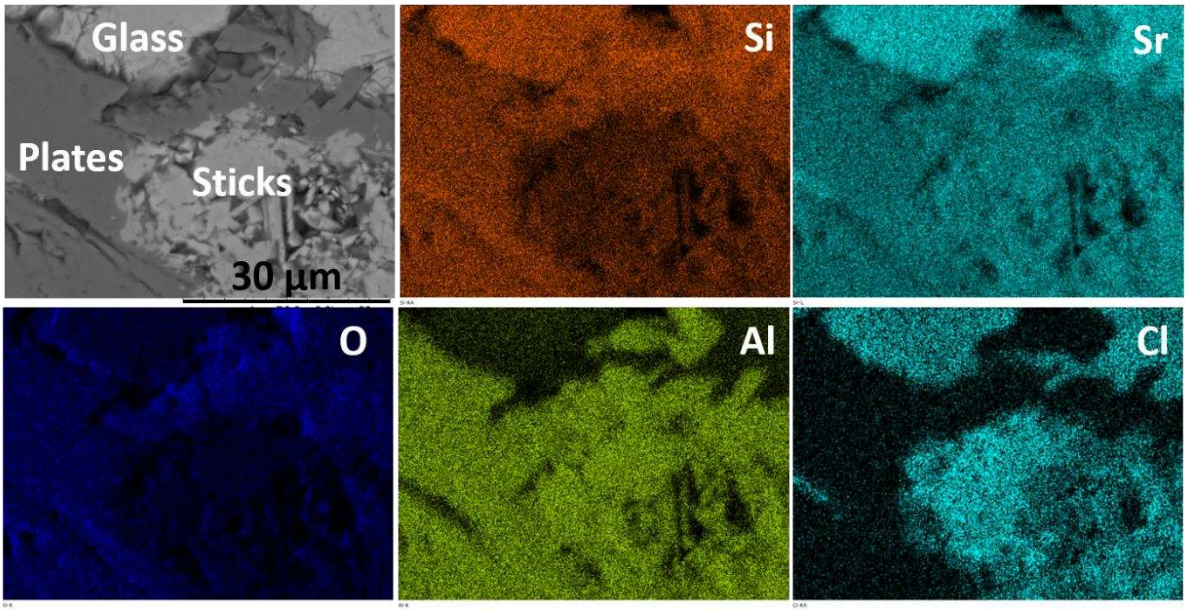

Fig. 15 Elemental mapping of the separated phases in SAS-25Cl glass.

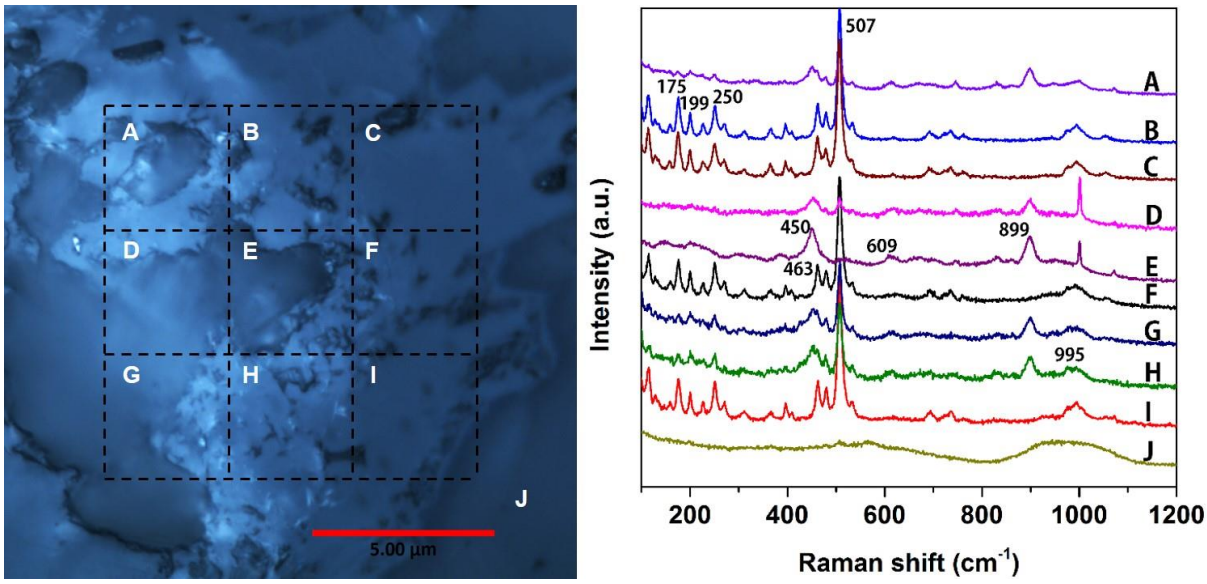

Fig. 16 Micro-Raman spectra of separated phases in SAS-25Cl glass.